Lattice Boltzmann Study of the Geometric Effect of a Perforated Orifice on Its Damping Performance

Chenzhen JI[1]; Dan ZHAO[1,2]; Shihuai LI[1]; Xinyan Li[1]

[1] Aerospace Engineering Division, College of Engineering, Nanyang Technological University, Singapore, 639798

ABSTRACT

The present work considers the geometric effect of a perforated orifice on its noise-damping performance by conducting 2D lattice Boltzmann simulations. The damping effect of a rounded orifice is characterized by using power absorption coefficient by applying an acoustically-excited flow consisting of multiple tones. Comparison is then made between the damping performance of the rounded orifice and a square one. It is found that the rounded orifice is associated with lower damping effect than that of the square one. This is due to the different intensity vorticities generated, as visualized in the vortex shedding contours. To gain further insight on the damping mechanism and performance of the orifices, the orifice thickness effect is studied. As the orifice diameter remains constant, the damping performance of the orifices becomes deteriorates in terms of the effective frequency bandwidth with the increased thickness. The present work confirms the effect of the orifice shape and geometry plays an important role in its noise-damping performance.

Keywords: Acoustic liner, Perforated orifices I-INCE Classification of Subjects Number(s): 21.6

1. INTRODUCTION

Thermoacoustic instability(1) is generated by the interaction between unsteady heat release and acoustic waves. Its occurrence can cause many plaguing problems such as mechanical failure, large amplitude noise and increase heat release rate on the aero-engines. To mitigate combustion instabilities, the coupling between unsteady heat release and acoustic waves must somehow be interrupted(2). Perforated liners along the bounding walls of a combustor are widely used as acoustic dampers(3, 4, 5, 4, 6)to dissipate the acoustic waves. They are usually made by metal sheets, which have tiny orifices in them. In practice, a cooling air flow through the orifices (known as bias flow) is needed to prevent the liners from being damaged under high temperature. Over the last few decades, perforated liners have been the subject of intense research activity, aiming to better understand and predict their damping performance.

To shed lights on their damping mechanism and to predict their damping, lots of investigations of orifices are widely conducted. Howe(7) modeled the acoustic energy dissipated by the periodic shedding of vorticity for a single orifice at a high Reynolds-number by using Rayleigh conductivity. Eldredge & Dowling(8) recently developed a 1D duct model in frequency domain to simulate the absorption of axial plane wave by a double-liner with a bias flow. The damping mechanism of vortex shedding was embodied using a homogeneous liner compliance adapted from the Rayleigh conductivity. Due to the high performance computer and more efficient computational methods, numerical simulation becomes more popular. Tam *et al.*(9) carried out direct numerical simulation (DNS) of a single aperture, showing that vortex shedding was the dominant mechanism of absorption for incident waves of high amplitude. Mendez & Eldredge(10) conducted compressible large-eddy simulations (LES) in time domain to study the flow through a single perforated hole or multiple holes. Ji & Zhao(11) investigated the acoustics behavior in a 3D acoustic liner using lattice Boltzmann method and found that vorticity generation and shedding were affecting the sound absorption ability of the liner.

The need to improve perforated liners designs with current low-emission engines leads to a resurgence of liner focused research. The perforation geometry has been observed to have a significant influence on the aeroacoustic response of wall perforations. Jing & Sun's(12) experiments showed that the thickness and the bias flow Mach number play the dominant roles in affecting the liners' performance. Kooijman *et al.*(13) investigated the influence of the edge geometry of a slit shaped perforation subjected to pure grazing flow. The amplitudes of the oscillations in resistance and reactance were observed to be larger for sharp edged

[2] zhaodan@ntu.edu.sg

geometries. Lahiri *et al*.(14) investigated the effect of several parameters on the damping performances of perforated liners subjected to a grazing-bias flow combination. Wall perforations with chamfered edges, compared to sharp edges, were observed to lead to higher resistance, at low Strouhal numbers. Tonon *et al*.(15) experimentally investigated the effect of grazing flow on the impedance of slit shaped wall perforations by means of a multi-microphone impedance tube. The flow on the perforation impedance was observed to be sensitive to the perforation geometry.

Most of optimum design of works on acoustic liner geometry were done by experiments. However, detailed flow and acoustic signature investigations on the acoustic liner are not easy to conduct. Because of small-size orifice (typically around 1 mm in diameter), both specific geometry manufacture and flow field observing in and around the orifice are difficult to obtain. Meanwhile, computational fluid dynamics (CFD) can be used as an effective tooling since it can overcome those weakness on the experiments. In this work, we conduct numerical simulation to investigate the effect of two kinds of orifice geometry (rounded and square) on the damping performance of acoustic liner, and analyze the mechanism through the voricity generation and shedding. In addition, the plate thickness is also studied as an important factor.

The presented paper is organized as follows: in Sect. II, the numerical scheme and configuration are presented. In Sec. III, definition of the sound absorption coefficient is described to characterize the acoustic damping of the orifice. In Sect. IV, geometry configuration and thickness effecting on the acoustic performance is performed in the presence of a bias flow.

2. NUMERICAL SCHEME AND CONFIGURATION

2.1 Lattice Boltzmann Equation

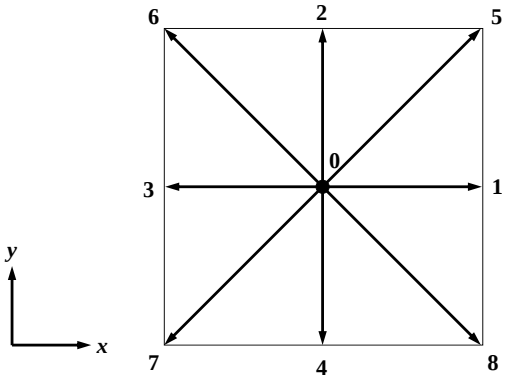

Figure 1 – Two-dimension, nine-velocity (D2Q9) lattice model.

Unlike conventional numerical schemes, LBM is classified as a particle technique. It simulates the space-temporal evolution of fluid field based on a time-space discretization of the Boltzmann equation, known as the lattice Boltzman equation (LBE). The LBE controls the particles associated with collision and propagation over a discrete lattice mesh. The conserved variables such as density, momentum and internal energy are obtained by performing a local integration of the particle distribution. Compared with Navier-Stokes solvers, LBM is easier to implement and code, more successful in dealing with complex boundaries and with the potential for parallelization. Thus it has been applied to study not only fluid flows but also aeroacoustics, such as jet, cavity and airfoil noise. Much of the previous works(16) has concluded that LBM possesses the required accuracy to capture weak acoustic pressure fluctuations.

LBM originated from lattice gas automata, is based on mesoscopic models and kinetic equations. Simplified kinetic models are developed that assume the fluid flow composes of a collection of pseudo-particles. They can be represented by a set of density distribution functions. These particles are associated with collision and propagation over a discrete lattice mesh. In order to perform particles motions, the fluid domain is discrete into a specific group by series of nodes and lattices, depending on the different models.

Fig. 1 depicts the lattice model used in this work, known as D2Q9, and it means a particle has nine feasible discrete propagation directions in each node and the motion occurs in two dimensional space. The discrete velocity vectors $\boldsymbol{e}_i$ set of the particles for the D2Q9 model, are defined as:

$$\boldsymbol{e}_i = \begin{cases} 0, \quad i = 0, \\ c_l(\cos(\frac{i-1}{4}\pi), \quad \sin(\frac{i-1}{4}\pi)), \quad i = 1,3,5,7, \\ \sqrt{2}c_l(\cos(\frac{i-1}{4}\pi), \quad \sin(\frac{i-1}{4}\pi)), \quad i = 2,4,6,8, \end{cases} \tag{1}$$

where $c_l = \Delta x/\Delta t$ (lattice space/time step) is the particle propagation speed on the lattice, taken as $c_l = 1$ in most cases.

The fundamental propagation and the collision of the fluid particles over the lattice are governed by a space-temporal discretization of the Boltzmann equation, which is also named as lattice Botlzmann equation, given by:

$$f_i(\boldsymbol{x}+\boldsymbol{e}_i\Delta t, t+\Delta t) - f_i(\boldsymbol{x},t) = -\frac{1}{\tau}(f_i(\boldsymbol{x},t) - f_i^{eq}(\boldsymbol{x},t)), \tag{2}$$

where f_i is the distribution function associated with the propagation direction i at the spatial coordinate $\boldsymbol{x}$ and time t. The single relaxation parameter τ defines particle collision and acts to control the kinematic viscosity of the fluid: $\nu = (2\tau - 1)/6$. f_i^{eq} is the equilibrium distribution function, which is the second order truncated expansion of the Maxwell-Boltzmann equilibrium function, expressed as:

$$f_i^{eq} = \rho w_i(1 + \frac{3}{c^2}\boldsymbol{e}_i\cdot\boldsymbol{u} + \frac{9}{2c^4}(\boldsymbol{e}_i\cdot\boldsymbol{u})^2 - \frac{3}{2c^2}\boldsymbol{u}\cdot\boldsymbol{u}), \tag{3}$$

where w_i is the weighting factor and given as:

$$w_i = \begin{cases} \frac{4}{9}, & i = 0, \\ \frac{1}{9}, & i = 1,2,3,4, \\ \frac{1}{36}, & i = 5,6,7,8. \end{cases} \tag{4}$$

The left hand side of the Eq. (2) represents the propagation operator and determines the diffusion of the distribution functions over the lattice. The right hand term of Eq. (2), known as Bhatnagar-Gross-Krook (BGK) collision operator(17), is a simplification of the collision function based on the use of a single relaxation time τ in all directions i. The local macroscopic variables ρ and $\boldsymbol{u}$ on each lattice site are obtained in terms of the local distribution function f_i by:

$$\rho(\boldsymbol{x},t) = \sum_{i=0}^{8} f_i(\boldsymbol{x},t), \tag{5}$$

$$\rho\boldsymbol{u}(\boldsymbol{x},t) = \sum_{i=0}^{8} \boldsymbol{e}_i f_i(\boldsymbol{x},t). \tag{6}$$

The equation of state is that of an ideal gas and thus $p = \rho c_s^2$, where the dimensionless speed of sound c_s in D2Q9 model is $1/\sqrt{3}$. By using the Chapman-Enskog expansion, the lattice Boltzmann equations can be recovered to the compressible Navier-Stokes equation at the hydrodynamic limit(18).

2.2 Turbulence modeling

For turbulence simulation, a common implementation is to combine the Smagorinsky(19) subgrid model into the collision term of lattice Boltzmann equation. Implementing the turbulent model involves two steps:
(a) Evaluation of the local stress tensor:

$$\prod_{m,n} = \sum_{i=0}^{8} \boldsymbol{e}_{i,m}\boldsymbol{e}_{i,n}(f_i - f_i^{eq}), \tag{7}$$

where $(m,n) \in \{x,y\} \times \{x,y\}$.
(b) Computation of the enhanced relaxation time:

$$\tau_e = 3(\nu + C^2 S) + 0.5, \tag{8}$$

where $S = (\sqrt{\nu^2 + 18C^2\sqrt{\prod_{m,n}\prod_{m,n}}} - \nu)/(6C^2)$ and the C is a Smagorinsky constant set as 0.18 in current simulation.

2.3 Non-reflection Boundary Condition

The inlet and outlet are treated with an absorbing boundary condition scheme (ABC) proposed by Kam *et al*(20).The concept of the ABC technique is very similar to the perfectly matched layer method commonly used in computational aeroacoustics scheme. It involves using a buffer zone between the fluid region and the outlet boundary to create an asymptotic transition towards a target flow in terms of target distribution function f_i^T. This is done by adding an extra term to Eq. (2), which becomes:

$$f_i(\boldsymbol{x}+\boldsymbol{e}_i\Delta t, t+\Delta t) - f_i(\boldsymbol{x},t) = -\frac{1}{\tau}(f_i(\boldsymbol{x},t) - f_i^{eq}(\boldsymbol{x},t)) - \sigma(f_i^{eq}(\boldsymbol{x},t) - f_i^{T}(\boldsymbol{x},t)), \tag{9}$$

where $\sigma = \sigma_T(\eta/\beta)^2$ is the absorption coefficient, $\sigma_T = 0.3$ is a constant, η is the distance measured from the beginning of the buffer zone and β is the thickness of the buffer. The f_i^T can be obtained in the same manner as the f_i^{eq} by using the Eq. (3). The non-reflecting condition is achieved by setting $\boldsymbol{u}_T = \boldsymbol{u}_0$ and $\rho_T = \rho_0$, where $\boldsymbol{u}_0$ and ρ_0 are the undisturbed velocity and density at the boundary. The thickness of the ABC buffer β used in presented work corresponds to 20 cells.

2.4 Numerical Configuration

In practice, perforate liners may consist of thousands of tiny size orifices. However, if the open area ratio is small enough, it can be assumed that there is no interaction of the voriticity between neighboring orifices. Thus the damping behaviors of single orifice can be used to predict the liners, as studied by Mendez and Eldredge(10).

The geometric configuration is illustrated in Fig. 2. An acoustically excited flow with a mean flow $\overline{u}$ and an oscillating velocity u' is forced to pass through an orifice with opening size d in a duct with width D. The thickness of plate is characterized as T. When the fluid is injected through the orifice, a bias flow is formed with a mean velocity approximate $\bar{U}$, and Reynolds number can be defined as $\mathrm{Re} = \rho\bar{U}d/\nu$. The inlet is located upstream at l from the plate, and the outlet is at L downstream. Here, L is chosen large enough to avoid spurious interactions between the outlet condition and the zone of computational interest.

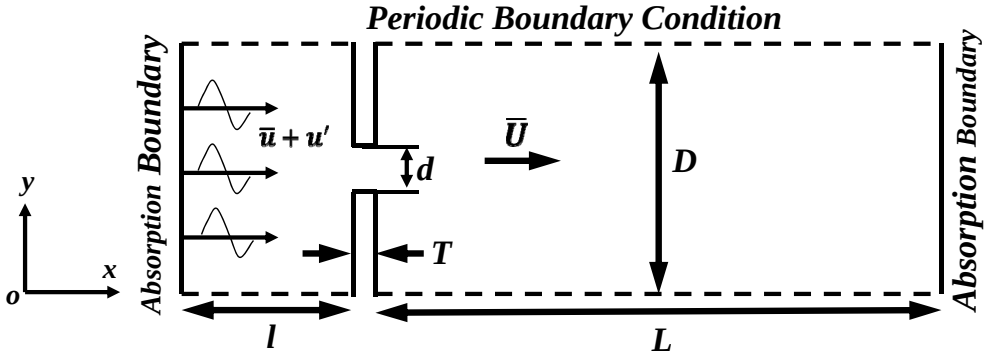

Figure 2 – Geometry of the liner with a square single orifice.

3. DEFINITION OF ABSORPTION COEFFICIENT DESCRIPTION

The acoustic damping of the orifice can be characterized by using power absorption coefficient, which describes the fraction of incident waves being absorbed. It is defined as:

$$\Delta = 1 - |R|^2, \tag{10}$$

where R is the reflection coefficient as given:

$$R = \frac{z_t + 1}{z_t - 1}. \tag{11}$$

Here, z_t is the normalized acoustic impendence of the whole system, and given as the sum of perforated liner impedance z_p and cavity impedance z_c:

$$z_t = z_p + z_c. \tag{12}$$

Assuming planar waves are propagating between the perforated plate and the back wall, the cavity impedance can be shown as:

$$z_c = -\mathrm{j}\cot(kl), \tag{13}$$

where $\mathrm{j} = \sqrt{-1}$ and k is the acoustic wave number and l is the cavity depth. The impedance of the perforated plate is defined as:

$$z_p = \frac{\tilde{p}_d - \tilde{p}_u}{\tilde{u}_0}, \tag{14}$$

where c is the speed of sound, $\tilde{u}_0$ is velocity fluctuations at the center of the orifice, $\tilde{p}_d$ and $\tilde{p}_u$ are the pressure fluctuations at the downstream and upstream of the orifice, respectively.

Then, The total impedance of the system is obtained:

$$z_t = z_p + z_c = \frac{\tilde{p}_d - \tilde{p}_u}{\tilde{u}_0} - \mathrm{j}\cot(kl). \tag{15}$$

substituting Eqs. (11) and (15) into Eq. (10), power absorption coefficient can then be calculated.

4. RESULTS AND DISCUSSION

Before we use the model, validations are conducted by comparing our numerical results with the analytical ones. Note that the analytical results are obtained by conducting frequency-domain analysis of a square orifice. For comparison, the numerical configuration is illustrated as in Fig. 2. And the geometric parameters are set as: $T = 2$ mm, $d = 6$ mm, $D = 50$ mm, $l = 35$ mm and $L = 105$ mm. The acoustically excited bias flow consisting of multiple tones is set as:

$$u_{in}(t) = \bar{u} + u' = 0.5 + 0.005 \sum_{k=1}^{28} \sin(2\pi f_k t), \tag{16}$$

where f is the forcing frequency. It can be seen that the acoustically excited flow covers a broad frequency range (31.83 to 891.27 Hz) in increments of 31.83 Hz. The present simulation is conducted in time-domain. And it is is different from frequency domain simulation, of which the liner's damping is characterized one frequency at a time. These frequencies correspond to a range of Strouhal numbers St from 0.11 to 3.05, corresponding to the mean bias flow velocity $\bar{U} \approx 5.5$ m/s.

Fig. 3 (a) illustrates the variation of the power absorption coefficient with Strouhal number. The absorption is maximum around $f \approx 350$ Hz, resulting in an absorption peak approaching 1.0. At this frequency, almost all the incident acoustic aves are absorbed. Comparison is then made between the present model, Howe's model (HM) and modified Howe's model (MHM). Good agreement between LBM and MHM is also found, although HM predicts a larger damping at high frequency. And Fig. 3 (b) shows the consistent results by the phase of reflection coefficient.

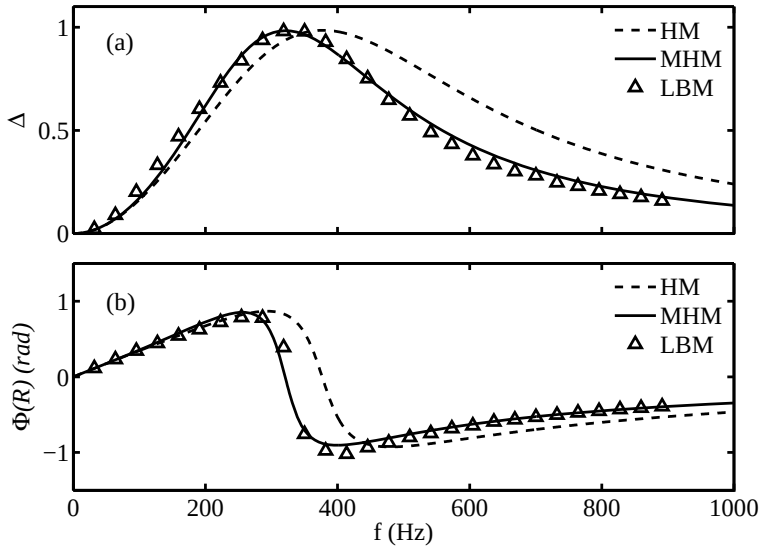

Figure 3 – Comparison between results from lattice Boltzmann method (LBM), Howe model (HM) and modified Howe model (MHM): (a) Sound absorption coefficient Δ; (b) phase of the reflection coefficient $\Phi(R)$.(21)

4.1 Orifice Shape Effect

To investigate the orifice shape effect on the sound absorption property, two different plate shapes are simulated and compared: square and rounded. The radius of the semi-cycle at the rounded orifice is characterized as r, and $2r = T$, where T is the plate thickness. The details of geometry comparison are described in Fig. 4 and the numerical setting up keeps consistent as used in section 4.1. From the results comparison of the sound absorption coefficient illustrated in Fig. 5, it can observed that the maximum sound absorption coefficient from the liner with the rounded orifice Δ^r_{max} is about 0.9, which is lower than the $\Delta^s_{max} \approx 1.0$ from the square one. And the effective bandwidth is also narrower when using the rounded orifice. It indicates that the liner with rounded orifice has poorer sound absorption ability than the one using the square orifice.

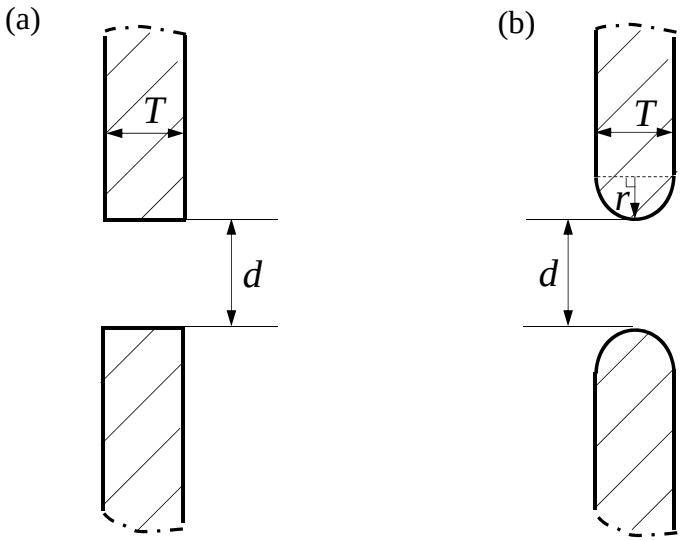

Figure 4 – Geometry comparison of the square (a) and rounded (b) orifice liner.

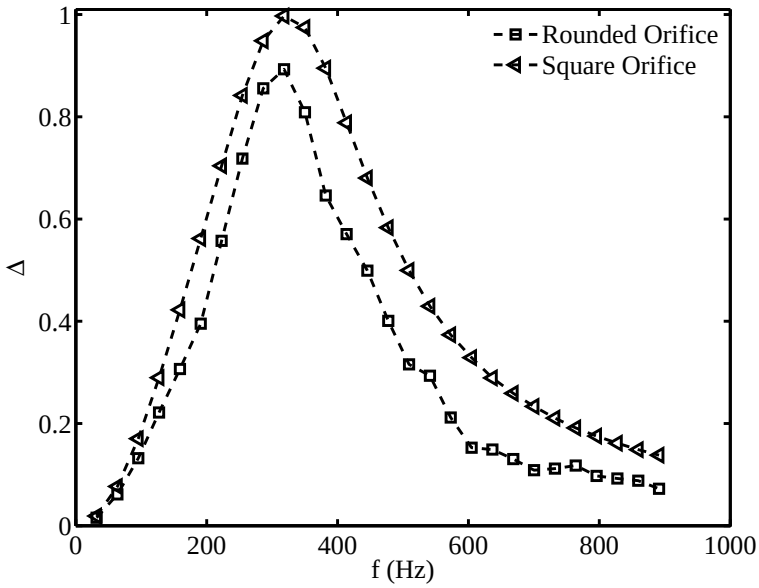

Figure 5 – Sound absorption coefficient comparison between the square and rounded orifice liner.

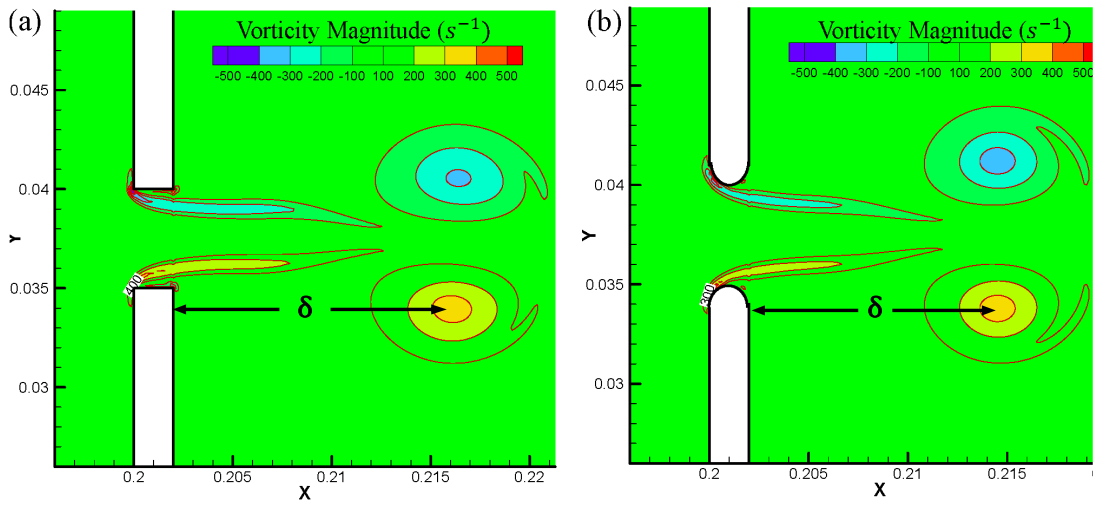

Figure 6 – Vorticity magnitude of the square (a) and rounded (b) orifice liner.

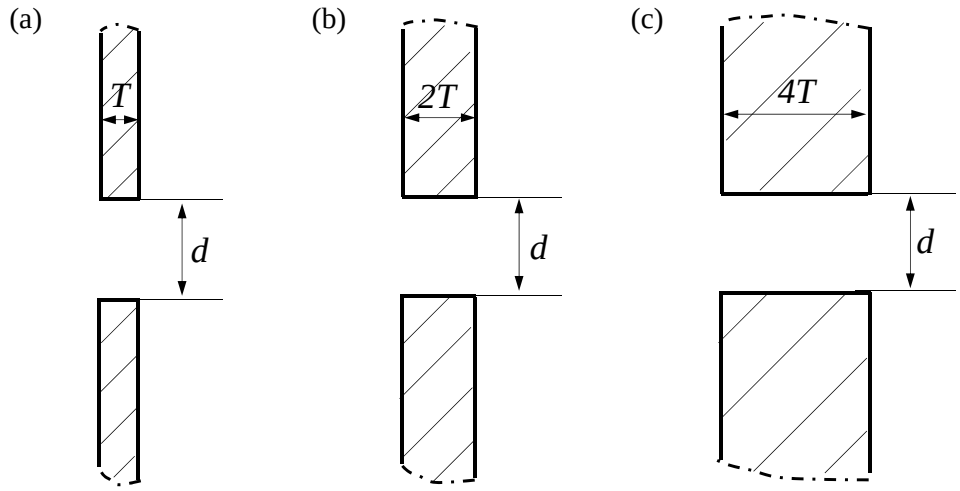

Figure 7 – The regular orifice liner with three kinds of plate thickness: (a) T; (b) 2T; (c) 4T.

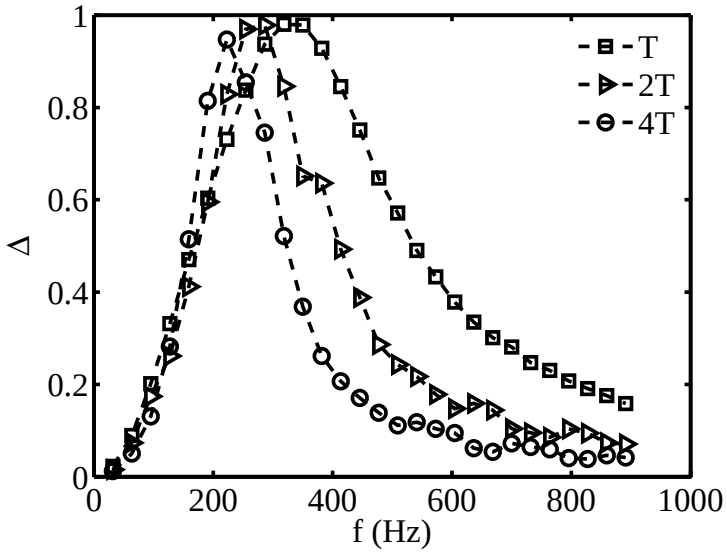

Figure 8 – The regular orifice liner with three kinds of plate thickness: (a) T; (b) 2T; (c) 4T.

To better understand the mechanism causing the difference in sound absorption, another numerical simulation is conducted by adding a periodic flow fluctuation at upstream without mean flow ($\bar{u} = 0$) as given:

$$p' = |p| \sin(2\pi f t), \tag{17}$$

where $|p|$ and f are the amplitude and frequency of the perturbation respectively. $|p|$ equals to the 0.01% of the atmospheric pressure, and frequency f is set to 318Hz. When the excited acoustic wave from the upstream pass through the orifice, part of acoustic energy is used to generate the vortex at the edge of orifice and make them shedding to the downstream. That explains why the orifice can dissipate the sound in a lined duct. Fig. 6 (a) and (b) show the vortex shedding from the square and rounder orifice, respectively. For comparison, both of them are recorded at the same flow time. It can be seen that the intensity of vorticity generated at rounded orifice is $\mathrm{I}_r = 300s^{-1}$, which is less than $\mathrm{I}_s = 400s^{-1}$ from the square one. And the shedding distance of vortex $\delta_r < \delta_s$ also indicates that the more acoustic energy is transformed to kinetic energy for vortex motion when through the square orifice.

4.2 Orifice Thickness Effect

It has been shown in the previous experiments that plate thickness also has a major influence on the acoustic properties of a liner with bias flow(12). Particular attention is now paid to the evaluation of the effect of finite plate thickness on its acoustic absorption property. In the presence of a same bias flow $\bar{U} \approx 5.5$ m/s, the

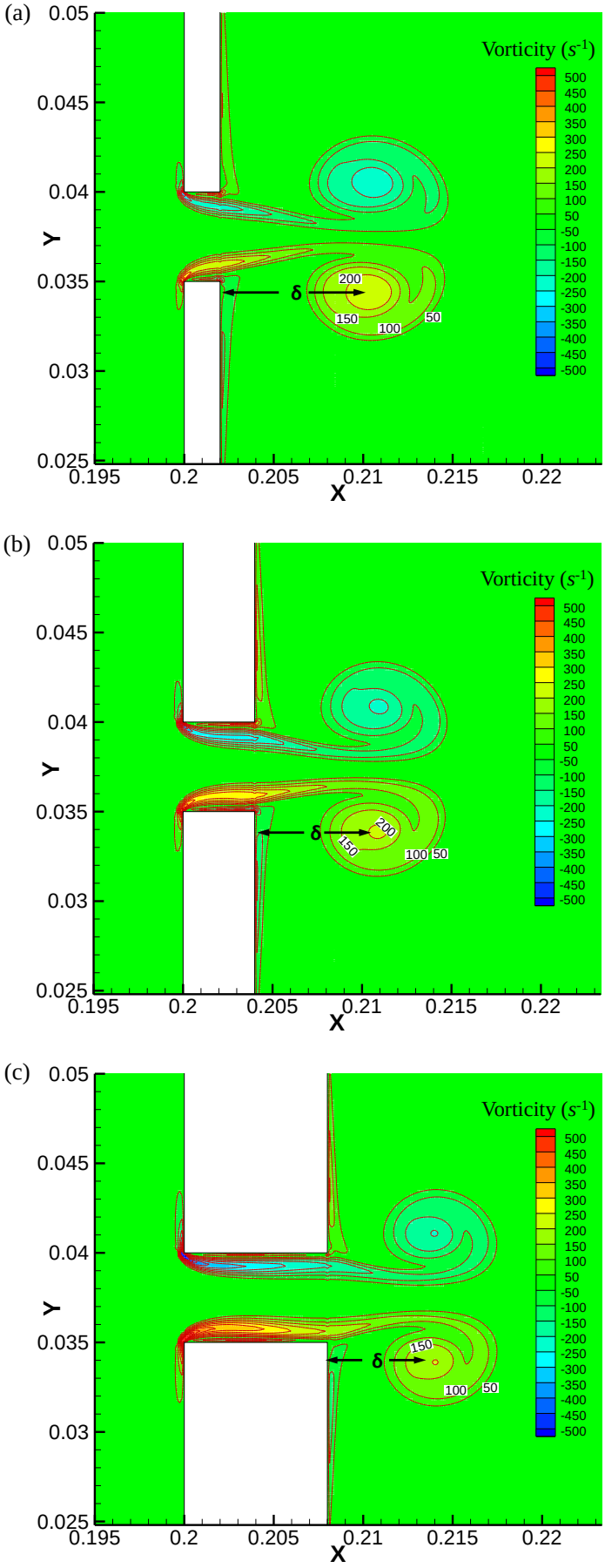

Figure 9 – Vorticity shedding contour for the different plate thickness: (a) T; (b) 2T; (c) 4T.

absorption coefficients of a perforated plate are calculated in three different thickness T(2mm), 2T and 4T shown in Fig. 7. As the thickness increases from T to 4T, the maximum sound absorption coefficient Δ_{max} varies little, however, the frequency of maximum absorption changes obviously and the effective bandwidth becomes narrower as shown in Fig. 8. Vortex shedding is also recorded at the same flow time during the simulation as done in section 4.2. The vortex intensity and shedding distance are marked on the Fig. 9. By comparing the vortex intensity I_T, I_{2T} and I_{4T}, it can be clearly seen that the I_T is strongest among them. And the distance that vortex sheds from the downstream edge of the plate δ_T is the longest. It can be explained vortex I_{4T} generated at the upstream edge of the orifice loses most energy on the boundary layer as it has to go through the thickest plate thickness(4T).

5. CONCLUSIONS

2D numerical simulations of the damping performance of a rounded and a square orifice are conducted. The model is developed in time domain by solving the discrete lattice Boltzmann equations via using the pseudo-particle based technique. It controls the particles associated with collision and propagation over a discrete lattice mesh. Acoustic variables such as pressure, density and internal energy are determined by performing a local integration of the particle distribution at each time step. This is different from the conventional numerical models attempting to solve Navier-Stokes equations by using high-order finite difference or finite volume methods. In order to enable the orifice damping performance to be characterized over a broad frequency range, acoustically-excited flow consisting of multiple tones is applied to the orifices. Here we use power absorption coefficient as the damping performance indicator. It describes the fraction of incident waves being absorbed. It is shown that the rounded orifice is associated with lower damping effect than that of the square one. This is due to the reduced intensity vorticities generated, as visualized in the vortex shedding contours. Further investigations reveal that the orifice thickness also plays a critical role in determine the orifice damping performance. As the orifice diameter remains constant, the maximum power absorption of the square or rounded orifice and its effective frequency bandwidth are decreased with the increased thickness. The present work confirms the effect of the orifice shape and geometry on determining its noise-damping performance.

ACKNOWLEDGEMENTS

The work is supported by Singapore Ministry of Education, ACR-Tier1-GR91/13-M4011228. The financial support is gratefully acknowledged.

REFERENCES

1. Richards GA, Straub DL, Robey EH. Passive control of combustion dynamics in stationary gas turbines. Journal of Propulsion and Power. 2003;19(5):795–810.

2. Zhao D, Morgans AS. Tuned passive control of combustion instabilities using multiple Helmholtz resonators. Journal of sound and vibration. 2009;320(4):744–757.

3. Zhao D. Transmission loss analysis of a parallel-coupled Helmholtz resonator network. AIAA journal. 2012;50(6):1339–1346.

4. Zhao D. A real-time plane-wave decomposition algorithm for characterizing perforated liners damping at multiple mode frequencies. The Journal of the Acoustical Society of America. 2011;129(3):1184–1192.

5. Zhao D, Morgans AS, Dowling AP. Tuned passive control of acoustic damping of perforated liners. AIAA journal. 2011;49(4):725–734.

6. Zhong Z, Zhao D. Time-domain characterization of the acoustic damping of a perforated liner with bias flow. The Journal of the Acoustical Society of America. 2012;132(1):271–281.

7. Howe M. On the theory of unsteady high Reynolds number flow through a circular aperture. Proceedings of the Royal Society of London A Mathematical and Physical Sciences. 1979;366(1725):205–223.

8. Eldredge JD, Dowling AP. The absorption of axial acoustic waves by a perforated liner with bias flow. Journal of Fluid Mechanics. 2003;485:307–335.

9. Tam CK, Kurbatskii KA, Ahuja K, Gaeta Jr R. A numerical and experimental investigation of the dissipation mechanisms of resonant acoustic liners. Journal of Sound and Vibration. 2001;245(3):545–557.

10. Mendez S, Eldredge JD. Acoustic modeling of perforated plates with bias flow for large-eddy simulations. Journal of Computational Physics. 2009;228(13):4757–4772.

11. Ji C, Zhao D. Lattice Boltzmann investigation of acoustic damping mechanism and performance of an in-duct circular orifice. The Journal of the Acoustical Society of America. 2014;135(6):3243–3251.

12. Jing X, Sun X. Experimental investigations of perforated liners with bias flow. The Journal of the Acoustical Society of America. 1999;106(5):2436–2441.

13. Kooijman G, Hirschberg A, Golliard J. Acoustical response of orifices under grazing flow: Effect of boundary layer profile and edge geometry. Journal of Sound and Vibration. 2008;315(4):849–874.

14. Lahiri C, Enghardt L, Bake F, Sadig S, Gerendás M. Establishment of a high quality database for the acoustic modeling of perforated liners. Journal of Engineering for Gas Turbines and Power. 2011;133(9):091503.

15. Tonon D, Moersy EMT. Aeroacoustics of a wall perforation in the pure grazing flow regime: effect of the perforation geometry. AIAA Paper. 2012;(2054).

16. Marié S, Ricot D, Sagaut P. Comparison between lattice Boltzmann method and Navier–Stokes high order schemes for computational aeroacoustics. Journal of Computational Physics. 2009;228(4):1056–1070.

17. Bhatnagar PL, Gross EP, Krook M. A model for collision processes in gases. I. Small amplitude processes in charged and neutral one-component systems. Physical review. 1954;94(3):511.

18. Chen H, Chen S, Matthaeus WH. Recovery of the Navier-Stokes equations using a lattice-gas Boltzmann method. Physical Review A. 1992;45(8):R5339.

19. Smagorinsky J. General circulation experiments with the primitive equations: I. The basic experiment*. Monthly weather review. 1963;91(3):99–164.

20. S Kam EW, C So RM, K Leung RC. Lattice Boltzman Method Simulation of Aeroacoustics and Nonreflecting Boundary Conditions. AIAA journal. 2007;45(7):1703–1712.

21. Ji C, Zhao D. Numerical Investigation of Acoustically Excited Flow Through an Orifice Using Lattice Boltzmann Method. AIAA Paper. 2013;(2127).